

# A Mixed Action Analysis of $\eta$ and $\eta'$ Mesons



K. Ottnad, C. Urbach, F. Zimmermann  
for the ETM Collaboration

---

## Abstract

We study  $\eta$  and  $\eta'$  mesons and their mixing angle in a mixed action approach with so-called Osterwalder-Seiler valence quarks on a Wilson twisted mass sea. The gauge configurations have been generated by ETMC for  $N_f = 2 + 1 + 1$  dynamical quark flavours and for three values of the lattice spacing. The main results are that differences in between the mixed action and the unitary approach vanish towards the continuum limit with the expected rate of  $\mathcal{O}(a^2)$ . The individual size of the lattice artifacts depends, however, strongly on the observable used to match unitary and valence actions. Moreover, we show that for the  $\eta$  mass valence and valence plus sea quark mass dependence differ significantly. Hence, in this case a re-tuning of the simulation parameters in the valence sector only is not sufficient to compensate for mismatches in the original quark masses.

*Key words:* arXiv:1501.02645, Lattice QCD; mixed action; Osterwalder-Seiler; pseudoscalar flavor-singlet mesons

*PACS:* [2010] 11.15.Ha, 12.38.Gc, 14.40.Df, 14.40.-n

---

## 1 Introduction

*Mixed action* approaches, where valence and sea fermion actions are chosen differently, are used frequently in lattice QCD. They possess a number of important advantages compared to the so-called *unitary* case, where valence and sea quark actions are identical. In particular, it might be possible to use a valence action obeying more symmetries than the sea action in cases where the valence action cannot be used in the sea for theoretical reasons or because of too high computational costs [1]. Prominent examples are overlap [2,3,4]

or domain wall [5] valence quarks on a Wilson-like or staggered sea. Concrete examples can be found for instance in Refs. [6,7,8].

When working in a mixed action approach, valence and sea actions need to be matched appropriately, for instance by tuning the valence quark masses such that a choice of meson masses agrees between unitary and mixed approaches. People even go one step further and try to correct for small mismatches in bare parameters used in the sea by using a partially quenched mixed action approach. The most extreme example for this approach is to use valence strange and charm on gauge configurations with only  $N_f = 2$  light dynamical quark flavours. In this case sea and valence actions are not matched, but the valence parameters are tuned such as to reproduce a choice of physical observables.

This ansatz has the big advantage that the gauge configurations do not need to be re-generated. However, while apparently quite successful, it is questionable whether this procedure works for observables with a strong sea quark dependence. Due to OZI suppression there are not many examples of such observables. But their very existence makes a clear distinction between QCD and the naive quark model.

Of course, a mixed action approach has also disadvantages, most prominently the breaking of unitarity, which might for instance drive certain correlators negative [9,10]. Also, it is not clear a priori how big lattice artifacts one encounters in mixed formulations.

In this paper we will present results on a particular mixed action approach with so-called Osterwalder-Seiler [11] valence quarks on an  $N_f = 2 + 1 + 1$  flavour Wilson twisted mass sea [12]. This particular action combination has the advantage that exact valence quark flavour symmetry is preserved. Moreover, the respective zero modes of sea and valence quarks coincide in the chiral limit. However,  $\mathcal{O}(a^2)$  violations of flavour (and parity) stemming from the sea quarks are still reflected in the magnitude of lattice artifacts on various physical observables.

As physical example we study the  $\eta$  and  $\eta'$  system. The large mass splitting observed among  $M_{\pi^0} \ll M_\eta \ll M_{\eta'}$  is thought to be due to the  $U_A(1)$  anomaly, a relation established via the Witten-Veneziano formula [13,14,15]. This lets one expect a significant dependence on the sea quark degrees of freedom. Speaking more technically, the corresponding correlation functions obtain significant contributions from fermionic disconnected diagrams and are, therefore, uniquely sensitive to differences between valence and sea formulations. Note that this was also discussed in the context of the validity of the fourth root trick in staggered simulations, see Refs. [16,17] and references therein.

After matching valence and sea actions, we compare observables extracted from unitary and valence operators. The unitary observables have been com-

puted in Refs. [18,19]. We study the continuum limit with different matching conditions and find remarkably good agreement to the unitary case. However, when comparing the valence with valence plus sea strange quark mass dependence of  $M_\eta$  we find significant differences.

These findings are important for future lattice QCD investigations: there are many phenomenologically interesting quantities involving flavour singlet pseudo-scalar mesons, for instance form factors of  $B$  or  $D_s$  decays to  $\eta\ell\nu$ . And maybe most prominently, there are anomaly related form factors of  $\eta \rightarrow \gamma\gamma$ , which can be used to estimate the light-by-light contribution to the hadronic part in the anomalous magnetic moment of the muon, in which we currently observe a deviation between theory and experiment at the few  $\sigma$  level [20,21,22,23]. The usage of Wilson twisted mass fermions described in this paper has significant advantages compared to other lattice actions due to a powerful variance reduction. And the possibility to use a mixed action will further ease those computations.

More generally, the findings here show that with a mixed action approach one can deal with fermionic disconnected diagrams, provided one applies an appropriate matching procedure. These disconnected diagrams become more and more important as they need to be treated appropriately for instance in investigations of hadron-hadron interactions. Since we show here that a mixed action approach works in the case of  $\eta, \eta'$  mesons, where the fermionic disconnected diagrams contribute significantly, we are confident that the same approach can be used for other physical observables. First accounts of this work can be found in Ref. [24]. Other studies of  $\eta$  and  $\eta'$  mesons from lattice QCD can be found in Refs. [17,25,26,27,28,29].

## 2 Lattice actions

The results we will present here are obtained by evaluating correlation functions on gauge configurations provided by the European Twisted Mass Collaboration (ETMC) [30]. We use the ensembles specified in table 1 adopting the notation from Ref. [30]. More details can be found in this reference.

The sea quark formulation is the Wilson twisted mass formulation with  $N_f = 2 + 1 + 1$  dynamical quark flavours. The Dirac operator for the light quark doublet reads [12]

$$D_\ell = D_W + m_0 + i\mu_\ell\gamma_5\tau^3, \quad (1)$$

where  $D_W$  denotes the standard Wilson Dirac operator and  $\mu_\ell$  the bare light twisted mass parameter.  $\tau^3$  and in general  $\tau^i, i = 1, 2, 3$  represent the Pauli matrices acting in flavour space.  $D_\ell$  acts on a spinor  $\chi_\ell = (u, d)^T$  and, hence, the  $u$  ( $d$ ) quark has twisted mass  $+\mu_\ell$  ( $-\mu_\ell$ ).

ensemble	$\beta$	$a\mu_\ell$	$a\mu_\sigma$	$a\mu_\delta$	$V$	$N_{\text{conf}}$	$N_b$
A40.24	1.90	0.0040	0.150	0.190	$24^3 \times 48$	1117	5
A60.24	1.90	0.0060	0.150	0.190	$24^3 \times 48$	1249	5
A80.24	1.90	0.0080	0.150	0.190	$24^3 \times 48$	2441	10
A100.24	1.90	0.0100	0.150	0.190	$24^3 \times 48$	968	5
A80.24s	1.90	0.0080	0.150	0.197	$24^3 \times 48$	2420	10
A100.24s	1.90	0.0100	0.150	0.197	$24^3 \times 48$	1196	5
B55.32	1.95	0.0055	0.135	0.170	$32^3 \times 64$	4450	5
D45.32sc	2.10	0.0045	0.0937	0.1077	$32^3 \times 64$	2220	10

Table 1

The gauge ensembles used in this study. For the labelling of the ensembles we adopted the notation in Ref. [30]. In addition to the relevant input parameters we give the lattice volume, the number of evaluated configurations  $N_{\text{conf}}$  and the block length  $N_b$  used for bootstrapping.  $N_b$  was chosen such that blocks cover at least 20 HMC trajectories of length one.

For the heavy unitary doublet of  $c$  and  $s$  quarks [31] the Dirac operator is given by

$$D_h = D_W + m_0 + i\mu_\sigma \gamma_5 \tau^1 + \mu_\delta \tau^3. \quad (2)$$

The bare Wilson quark mass  $m_0$  has been tuned to its critical value [32,30]. This guarantees automatic order  $\mathcal{O}(a)$  improvement [33], which is one of the main advantages of the Wilson twisted mass formulation of lattice QCD.

$\eta$  and  $\eta'$  masses have been computed in this framework in Refs. [18,19,34] on the same set of gauge configurations used here (and more) – we will refer to this framework as the *unitary approach*. However, in order to account for – and possibly benefit from – correlations we have re-evaluated the unitary  $\eta$  and  $\eta'$  masses on exactly the same gauge configurations as used in the present study.

The splitting term in the heavy doublet (2) introduces flavour mixing between strange and charm quarks which needs to be accounted for in the analysis. However, this complication can be avoided by using a mixed action approach for the valence strange and charm quarks. Formally, we introduce so-called Osterwalder-Seiler (OS) twisted valence strange and charm quarks [11,35]. The Dirac operator for a single valence quark flavour  $q$  reads

$$D_q = D_W + m_0 + i\mu_q \gamma_5. \quad (3)$$

Adapting the ideas of Ref. [11] to the  $\eta, \eta'$  system, we introduce two strange and two charm quark flavours,  $s, s'$  and  $c, c'$ , respectively. Flavours  $s$  and  $s'$  will have quark mass with equal modulus, but opposite sign:  $\mu_s = |\mu_s| = -\mu_{s'}$ , and the same for  $c$  and  $c'$ . Formally, the lattice action is extended to include a fermionic action corresponding to the Dirac operators (3) for all valence strange and charm quark flavours, accompanied by a ghost action to exactly cancel the contributions of the additional valence quarks to the fermionic

ensemble	$aM_K$	$aM_{\eta_s}$	$aM_{\pi_{\text{conn}}^0}$
A40.24	0.25884(43)	0.30708(60)	0.2375(25)
A60.24	0.26695(52)	0.31010(65)	0.2544(26)
A80.24	0.27706(61)	0.31406(46)	0.2659(25)
A100.24	0.28807(34)	0.31575(45)	0.2883(14)
A80.24s	0.25503(33)	0.27168(49)	0.2649(16)
A100.24s	0.26490(74)	0.27455(73)	0.2841(16)
B55.32	0.22799(34)	0.26087(33)	0.2177(10)
D45.32sc	0.17570(84)	0.21126(34)	0.1494(15)

Table 2

Values of the unitary kaon and  $\eta_s$  masses  $M_K$  and  $M_{\eta_s}$  in lattice units, which have been used to match mixed and unitary actions. In addition, we give the mass values  $M_{\pi_{\text{conn}}^0}$  of the connected neutral pion which becomes identical to  $\eta_s$  for mass degenerate light and strange quarks. This SU(3) symmetric situation is realised approximately for the A80.24s and A100.24s ensembles. The kaon mass data shown in this table has first been published in Ref. [18].

determinant. For details we refer to Ref. [11]. In this reference it was also shown that automatic  $\mathcal{O}(a)$ -improvement stays valid in this framework and unitarity is restored in the continuum limit. In particular, flavours  $s$  and  $s'$  ( $c$  and  $c'$ ) become identical.

It is important to notice that at finite lattice spacing values correlation functions involving  $s$  and  $s'$  ( $\mu_s = -\mu_{s'}$ ) differ by lattice artifacts. For instance, the masses extracted from the correlation function of the operator

$$\mathcal{O}_K^{\text{OS}} = \bar{\psi}_s i\gamma_5 \psi_d \quad (4)$$

where the fields  $\psi_q, \bar{\psi}_q$  denote single quark fields in the so-called physical basis, differ from the one extracted from the operator

$$\mathcal{O}_{K^0}^{\text{OS}} = \bar{\psi}_{s'} i\gamma_5 \psi_d \quad (5)$$

by  $\mathcal{O}(a^2)$  (we denote it with  $K^0$  in remedy of the neutral pion in the light sector). Only in the continuum limit these two masses will agree again.

Valence and unitary actions need to be matched appropriately. As shown in Ref. [11], in our case the matching can be performed in principle using the relation

$$\mu_{c/s} = \mu_\sigma \pm Z_P/Z_S \mu_\delta. \quad (6)$$

However, for the strange quark mass uncertainties in  $Z_P/Z_S$  are magnified in  $a\mu_s$ , and thus we decided not to rely on Eq. 6. Instead, meson masses are used: in previous studies it was found that matching kaon masses determined from the operator (4) to the unitary kaon masses is best in the sense that the residual lattice artifacts in the results computed in a mixed action approach are small [36]. We will call this procedure kaon matching.

For details on how to compute the kaon mass in the unitary case we refer to Ref. [37]. We note in passing that there is no kaon mass splitting introduced by the twisted mass formalism in the unitary case for the choice of a degenerate light quark doublet  $|\mu_u| = |\mu_d| = \mu_\ell$  [32].

As a second matching observable for the strange quark mass we use the mass of the so-called  $\eta_s$  meson  $M_{\eta_s}$ . The  $\eta_s$  is an artificial meson corresponding to the following interpolating operator

$$\mathcal{O}_{\eta_s}^{\text{OS}} = \bar{\psi}_s i\gamma_5 \psi_{s''} , \quad (7)$$

for which we assume  $\mu_s = \mu_{s''}$ , unlike the  $s'$  quark considered above, which had opposite sign. A benefit of this particular choice is the absence of disconnected diagrams in the corresponding two-point function. This procedure will be called  $\eta_s$  matching. For technical details, e.g. further interpolating fields and correlation functions we refer to section 3.

For both matching procedures on each gauge ensemble one tunes the value of  $a\mu_s$  such that the kaon or the  $\eta_s$  mass agrees within errors between the mixed and the unitary formulation. The unitary values of the masses we matched to are compiled in table 2. In order to compute the matching values for  $a\mu_s$  we performed inversions on a subset of the available configurations in a range of  $a\mu_s$  values and interpolated the squared OS meson masses linearly in  $a\mu_s$ . The matching values for  $a\mu_s$  for the two matching observables and all ensembles can be found in table 3. The values for  $M_K^{\text{OS}}$  and  $M_{\eta_s}^{\text{OS}}$  at the matching points are compiled in the appendix in table A.6. Note that in case of matching  $M_{\eta_s}$  we do not reach exact agreement for all ensembles within errors when recomputing  $M_{\eta_s}^{\text{OS}}$  from full statistics. These numerically small differences become irrelevant for the  $\eta$  and  $\eta'$  masses themselves due to the much larger statistical uncertainties introduced by the quark disconnected diagrams .

In the following we indicate quantities determined in the OS framework with the superscript <sup>OS</sup>, while quantities determined in the unitary case have no superscript. To distinguish the two matching procedures we use the superscripts <sup>K</sup> and  <sup>$\eta_s$</sup> .

As an example for the matching procedure we show in figure 1  $(aM_K^{\text{OS}})^2$ ,  $(aM_{\eta_s}^{\text{OS}})^2$  and  $(aM_{K^0}^{\text{OS}})^2$  as a function of the bare OS strange quark mass  $a\mu_s$  for the  $D45.32sc$  ensemble. In figure 1 the aforementioned OS kaon mass splitting can be observed. In the limit  $\mu_s = \mu_\ell$  this splitting corresponds to the difference between the charged pion mass and the connected only neutral pion mass. The splitting is almost independent of  $\mu_s$ , decreasing slightly with increasing  $\mu_s$ .

As expected,  $M_{\eta_s}$  is larger than the two kaon masses and agrees with  $M_{K^0}^{\text{OS}}$  in the limit  $\mu_s = \mu_\ell$ . All three squared masses show a linear dependence on  $\mu_s$ .

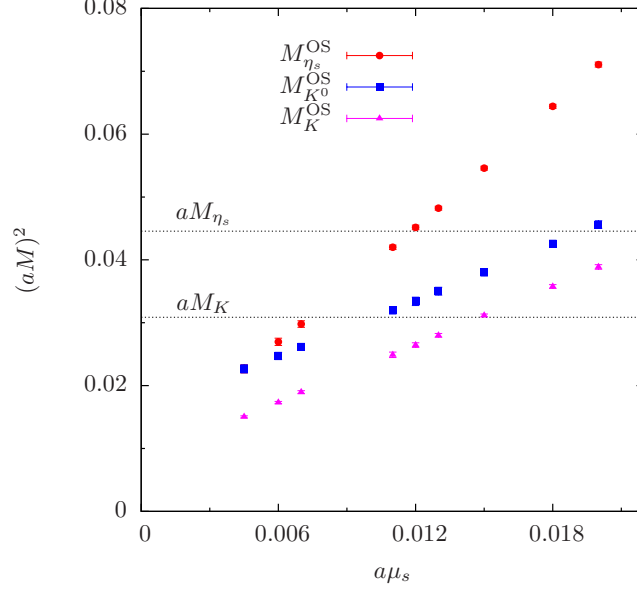


Fig. 1.  $(aM_K^{\text{OS}})^2$ ,  $(aM_{\eta_s}^{\text{OS}})^2$  and  $(aM_{K^0}^{\text{OS}})^2$  as a function of the bare OS strange quark mass  $a\mu_s$  for the  $D45.32sc$  ensemble. Horizontal lines indicate the unitary mass values that have been used for the matching.

ensemble	$a\mu_\ell$	$a\mu_s^K$	$a\mu_s^{\eta_s}$	$a\mu_c^K$
A40.24	0.0040	0.02300(25)	0.01239(25)	0.27700(25)
A60.24	0.0060	0.02322(22)	0.01303(22)	0.27678(22)
A80.24	0.0080	0.02328(20)	0.01338(20)	0.27672(20)
A100.24	0.0100	0.02381(21)	0.01380(22)	0.27619(21)
A80.24s	0.0080	0.01884(16)	0.00883(21)	0.28116(16)
A100.24s	0.0100	0.01877(22)	0.00922(23)	0.28123(22)
B55.32	0.0055	0.01858(12)	0.01100(10)	0.25142(12)
D45.32sc	0.0045	0.01488(30)	0.01180(12)	0.17252(30)

Table 3

Matching values of the OS valence strange quark masses  $\mu_s$  for kaon and  $M_{\eta_s}$  matching. The OS valence charm quark masses  $\mu_c^K$  have been determined using Eq. (8) for kaon matching only.

The horizontal lines indicate the corresponding unitary values that have been used for computing  $a\mu_s^K$  and  $a\mu_s^{\eta_s}$ .

For the charm quark mass the estimate from Eq. 6 is less affected by uncertainties. In order to circumvent the need for  $Z_P/Z_s$ , one can re-arrange Eq. 6 to

$$\mu_c = 2\mu_\sigma - \mu_s. \quad (8)$$

Because  $\mu_s \ll \mu_c$  and  $\eta, \eta'$  do not depend on  $\mu_c$ , we restrict ourselves to kaon matching for the  $\mu_s$  value entering the charm quark mass. The corresponding values for  $\mu_c \equiv \mu_c^K$  extracted in this way can be found in table 3.

All errors are computed using a blocked bootstrap procedure to account for

autocorrelation as well as all other statistical correlations in the data. The number of bootstrap samples was taken to be 1000 and the number of configurations per block  $N_b$  is given for every ensemble in table 1.  $N_b$  itself was chosen such that the length of a block corresponds to at least 20 HMC trajectories of length one. This value turned out sufficient to compensate for autocorrelation in the observables considered in this study.

### 3 Pseudo-scalar flavour-singlet mesons

In order to extract  $\eta$  and  $\eta'$  states we need a set of appropriate interpolating operators. As we are going to work in the quark flavour basis our choice is

$$\begin{aligned}\mathcal{O}_\ell^p(t) &= \frac{1}{\sqrt{2}} \sum_{\mathbf{x}} (\bar{\psi}_u i\gamma_5 \psi_u(\mathbf{x}, t) + \bar{\psi}_d i\gamma_5 \psi_d(\mathbf{x}, t)), \\ \mathcal{O}_s^p(t) &= \sum_{\mathbf{x}} \bar{\psi}_s i\gamma_5 \psi_s(\mathbf{x}, t), \\ \mathcal{O}_c^p(t) &= \sum_{\mathbf{x}} \bar{\psi}_c i\gamma_5 \psi_c(\mathbf{x}, t)\end{aligned}$$

in the physical basis, again denoted as  $\bar{\psi}_q, \psi_q$ . With Osterwalder-Seiler valence fermions we have to rotate the bilinears into the so-called twisted basis denoted as  $\bar{q}, q$ , see e.g. Ref. [38], in which also the Dirac operators in the previous section were written. Performing this axial rotation [12,11], one obtains the following operators in the so-called twisted basis

$$\begin{aligned}\mathcal{O}_\ell(t) &= \frac{1}{\sqrt{2}} \sum_{\mathbf{x}} (\bar{d}d(\mathbf{x}, t) - \bar{u}u(\mathbf{x}, t)), \\ \mathcal{O}_s(t) &= - \sum_{\mathbf{x}} \bar{s}s(\mathbf{x}, t), \\ \mathcal{O}_c(t) &= - \sum_{\mathbf{x}} \bar{c}c(\mathbf{x}, t).\end{aligned}$$

From these operators we build a correlation function matrix

$$\mathcal{C}(t)_{qq'} = \langle \mathcal{O}_q(t' + t) \mathcal{O}_{q'}^\dagger(t') \rangle, \quad q, q' \in \{\ell, s, c\}, \quad (9)$$

which allows us to obtain results for masses and amplitudes; cf. section 3.2.

The corresponding correlation functions have fermionic connected and disconnected contributions. The case for up and down quarks is like in the unitary approach and discussed in detail in Refs. [39,18,19]. Therefore, we concentrate on the disconnected contributions for strange and charm quarks. The correlation function of  $\mathcal{O}_s(t)$ , for instance, has the following contributions

$$\langle \mathcal{O}_s(t) \mathcal{O}_s^\dagger(0) \rangle_F = -\text{Tr}\{G_s^{0t} G_s^{t0}\} + \text{Tr}\{G_s^{tt}\} \cdot \text{Tr}\{G_s^{00}\}, \quad (10)$$



where  $\langle . \rangle_F$  denotes the average of fermions only and

$$G_s^{xy} = (D_s^{-1})(x, y) \quad (11)$$

denotes the strange OS propagator. The first term in Eq. 10 is the connected contribution and the second the disconnected one. Note that mixed flavour correlation functions have only disconnected contributions by definition. The ground state mass extracted only from the connected piece on the r.h.s. of Eq. 10 is the mass of the artificial  $\eta_s$  meson, which is employed for  $\eta_s$  matching.

We evaluate the connected only contribution to Eq. 10 using the one-end-trick [40]. In contrast to the Wilson case,  $\text{Tr}\{G_s^{0t}G_s^{t0}\}$  is in general complex valued. However, the imaginary part of the corresponding trace is a pure lattice artifact. This can be shown by considering a suitable combination of connected correlation functions involving OS quarks  $s$  and  $s'$

$$\begin{aligned} \langle \bar{\psi}_s i\gamma_5 \psi_s(x) \bar{\psi}_s i\gamma_5 \psi_s(0) - \{s \rightarrow s'\} \rangle_F &= \langle \bar{s}s(x) \bar{s}s(0) - \bar{s}'s'(x) \bar{s}'s'(0) \rangle_F \\ &= -\text{Tr}\{G_s^{0x}G_s^{x0}\} + \text{Tr}\{G_{s'}^{0x}G_{s'}^{x0}\} \\ &= -\text{Tr}\{G_s^{0x}\gamma_5(G_{s'}^{0x})^\dagger\gamma_5\} + \text{Tr}\{G_{s'}^{0x}\gamma_5(G_s^{0x})^\dagger\gamma_5\} \\ &= -\text{Tr}\{G_s^{0x}\gamma_5(G_{s'}^{0x})^\dagger\gamma_5\} + \text{Tr}\{G_s^{0x}\gamma_5(G_{s'}^{0x})^\dagger\gamma_5\}^\dagger \\ &= -2i \text{ImTr}\{G_s^{0x}\gamma_5(G_{s'}^{0x})^\dagger\gamma_5\} \\ &= -2i \text{ImTr}\{G_s^{0x}G_s^{x0}\}, \end{aligned}$$

where we have used the relation  $D_s = \gamma_5 D_{s'}^\dagger \gamma_5$  together with the cyclic property of the trace. Since the l.h.s. of the above relation vanishes in the continuum limit, we will drop the imaginary part in our calculations.

For the disconnected contribution to Eq. 10 we need to estimate  $\text{Tr}\{G_s^{tt}\}$  on every gauge configuration and all  $t$ -values.  $\text{Tr}\{G_s^{tt}\}$  is again in general complex valued. And again, one can show that the real part is a pure lattice artifact. Similar to the case of the connected contribution this can be inferred from the following equality

$$\begin{aligned} \langle -\bar{\psi}_s i\gamma_5 \psi_s(x) + \bar{\psi}_{s'} i\gamma_5 \psi_{s'}(x) \rangle_F &= \langle \bar{s}s(x) + \bar{s}'s'(x) \rangle_F \\ &= -\text{Tr}\{G_s^{xx}\} - \text{Tr}\{G_{s'}^{xx}\} \\ &= -\text{Tr}\{G_s^{xx}\} - \text{Tr}\{G_s^{xx}\}^\dagger \\ &= -2 \text{Re Tr}\{G_s^{xx}\}, \end{aligned}$$

which is zero in the continuum limit. Therefore, we will also drop the real part of the disconnected loops in the calculation. Similarly one can show that

$$\langle \bar{s}s(x) - \bar{s}'s'(x) \rangle_F = -2i \text{Im Tr}\{G_s^{xx}\}. \quad (12)$$

We remark that all of the above results hold for any further valence quark as well (e.g. the charm quark).

The full strange correlation function after subtraction of lattice artifacts is then given as

$$\langle \mathcal{O}_s(t) \mathcal{O}_s^\dagger(0) \rangle_F = -\text{ReTr}\{G_s^{0t} G_s^{t0}\} - \text{ImTr}\{G_s^{tt}\} \cdot \text{ImTr}\{G_s^{00}\}, \quad (13)$$

and analogously for the charm. Cross flavour terms involve only disconnected diagrams and are for instance given as

$$\langle \mathcal{O}_s(t) \mathcal{O}_c^\dagger(0) \rangle_F = -\text{ImTr}\{G_s^{tt}\} \cdot \text{ImTr}\{G_c^{00}\}. \quad (14)$$

### 3.1 Variance Reduction

The relation (12) enables us to use a very powerful variance reduction method developed originally for the disconnected contributions of the light doublet [39] also for strange and charm flavours (see also Ref. [41]). It is based on the identity (recall  $\mu_s = -\mu_{s'}$ )

$$D_s^{-1} - D_{s'}^{-1} = -2i\mu_s D_{s'}^{-1} \gamma_5 D_s^{-1}.$$

Therefore, using Eq. 12 we can estimate

$$\text{ImTr}\{G_s^{xx}\} = -\mu_s \text{Tr}\{G_{s'}^{xy} \gamma_5 G_s^{yx}\}, \quad (15)$$

and correspondingly for the charm quark. Following Ref. [39], we apply this variance reduction method also to the light doublet.

### 3.2 Matrix of Correlation Functions

By applying these results, we compute the matrix of Euclidean correlation functions in Eq. (9) and solve the generalised eigenvalue problem (GEVP) [42,43,44]

$$\mathcal{C}(t) v^{(n)}(t, t_0) = \lambda^{(n)}(t, t_0) \mathcal{C}(t_0) v^{(n)}(t, t_0), \quad (16)$$

for determining the meson masses  $M_\eta$ ,  $M_{\eta'}$  (and possibly  $M_{\eta_c}$ ) from the principal correlators  $\lambda^{(n)}(t, t_0)$ ,  $n \in \eta, \eta'$ . The effective masses are then computed by numerically solving

$$\frac{\lambda^{(n)}(t, t_0)}{\lambda^{(n)}(t+1, t_0)} = \frac{\exp^{-M_{\text{eff}}^{(n)} t} + \exp^{-M_{\text{eff}}^{(n)} (T-t)}}{\exp^{-M_{\text{eff}}^{(n)} (t+1)} + \exp^{-M_{\text{eff}}^{(n)} (T-(t+1))}}$$

for  $aM_{\text{eff}}^{(n)}$ . The matrix  $\mathcal{C}$  is enlarged to a  $6 \times 6$  matrix by using in addition fuzzed [45,40] operators.

At this point we recall that in the unitary case also the mass of the  $\eta_s$  is not obtained from a single correlation function but rather from the ground state of a correlation function matrix involving connected correlation functions for strange and charm quarks. This minor complication arises due to the violation of flavour symmetry in the Wilson twisted mass formulation and the fact that the action can no longer be chosen flavour-diagonal for a non-degenerate doublet. Therefore, one has to consider off-diagonal connected correlation functions in addition to the ones consisting only of strange and charm quarks. However, the off-diagonal connected contributions are a pure lattice artifact and in the continuum limit the expected behaviour is restored, i.e. strange and charm sector decouple regarding the connected pieces.

Apart from meson masses also matrix elements can be extracted from the GEVP, which are needed to obtain  $\eta$  and  $\eta'$  mixing angles. We define the mixing angles  $\phi_\ell$ ,  $\phi_s$  in the quark flavour basis using the pseudoscalar density matrix elements  $A_{q,n} = \langle 0 | \mathcal{O}_q | n \rangle$  with  $n \in \{\eta, \eta'\}$  and  $q \in \{l, s\}$  as

$$\begin{pmatrix} A_{\ell,\eta} & A_{s,\eta} \\ A_{\ell,\eta'} & A_{s,\eta'} \end{pmatrix} = \begin{pmatrix} c_\ell \cos \phi_\ell & -c_s \sin \phi_s \\ c_\ell \sin \phi_\ell & c_s \cos \phi_s \end{pmatrix}, \quad (17)$$

see also Refs. [18,19]. From chiral perturbation theory combined with large  $N_C$  arguments  $|\phi_\ell - \phi_s| / |\phi_\ell + \phi_s| \ll 1$  can be inferred according to Refs. [46,47,48,49] which is confirmed by lattice QCD [19]. Therefore, we will consider only the average mixing angle  $\phi$

$$\tan^2 \phi \equiv -\frac{A_{l,\eta'} A_{s,\eta}}{A_{l,\eta} A_{s,\eta'}}. \quad (18)$$

### 3.3 Excited State Removal

To improve the  $\eta'$  (and  $\eta$ ) mass determinations, we use a method first proposed in Ref. [50], successfully applied for the  $\eta_2$  (the  $\eta'$  in  $N_f = 2$  flavour QCD) in Ref. [39] and very recently to the  $N_f = 2 + 1 + 1$  case in Ref. [19]. It relies on the assumption that disconnected contributions are significant only for the  $\eta$  and  $\eta'$  state, but negligible for higher excited states. This means, in turn, that only the connected contributions to  $\mathcal{C}$  are affected by excited states.

Since the signal-to-noise ratio of the connected contributions is much larger than the one of the disconnected ones, we can determine the corresponding ground state at large Euclidean times and subtract the excited states at small times. This subtracted connected and the full disconnected contributions are combined in  $\mathcal{C}_{q,q'}^{\text{sub}}(t)$ , which is then used in the analysis. We refer to the discussion in Ref. [19] for more details.

This procedure clearly depends on the validity of the assumption. However, it

can be checked in our Monte-Carlo data: if the subtracted combination of connected and disconnected contributions does not show excited states anymore, we take it as a strong hint for the validity of the assumption. This is the case for all our ensembles, and it was also the case in the unitary approach [19].

For all ensembles we observe that the mass of the  $\eta$  meson is unaffected by this procedure within errors. Only the error estimates get significantly smaller. This is also the case for the  $\eta'$  where, however, the errors are quite significant before excited state removal.

As an example we show in figure 2 the effective masses of the two lowest-lying states for the  $A80.24s$  ensemble from  $\eta_s$  matching. The values shown in the left panel are obtained from the standard method using a  $6 \times 6$  correlation function matrix build from local and fuzzed operators, whereas the right panel shows the results for a  $3 \times 3$  local-only correlation function matrix with excited states removed from its connected contributions. Our fitted values are always obtained from a cosh-type fit to the respective principal correlators. The corresponding fit ranges are indicated by the bands in the plots. In general, our choice for the fit ranges  $[t_1, t_2]$  and the values of  $t_0$  for the GEVP are given in table A.7. We remark that – since there is usually no clear plateau reached for the  $\eta'$  state from the standard method – we apply a two-state fit to the corresponding principal correlator in this case. In all other cases we employed a single state fit in the plateau region.

Comparing the two panels in figure 2 one observes that the  $\eta$  mass plateau is unaffected, but starts at  $t/a = 2$  in the case of removed excited states. For the  $\eta'$  there is no plateau reached in the left panel before the signal is lost in noise, whereas in the right one a reasonable plateau is visible. The extracted masses still agree within errors.

## 4 Results

In order to compare the mixed case with the unitary case we match the two actions as detailed in the previous sections using either the kaon or the  $\eta_s$  mass. Next we compute OS meson masses at these matching points. As an example we show in figure 3 the effective masses for the principal correlators  $\lambda^{(n)}(t, t_0)$  of  $\eta$  and  $\eta'$  as a function of  $t/a$  after removal of excited states from the connected contributions. For  $\eta$  and  $\eta'$  a plateau in the effective masses is visible from early  $t/a$  on. The corresponding result of an exponential fit is indicated by the horizontal lines. The fit range corresponds to the extension of the lines in  $t/a$ . All OS meson masses are compiled in the appendix in tables A.1 and A.2.

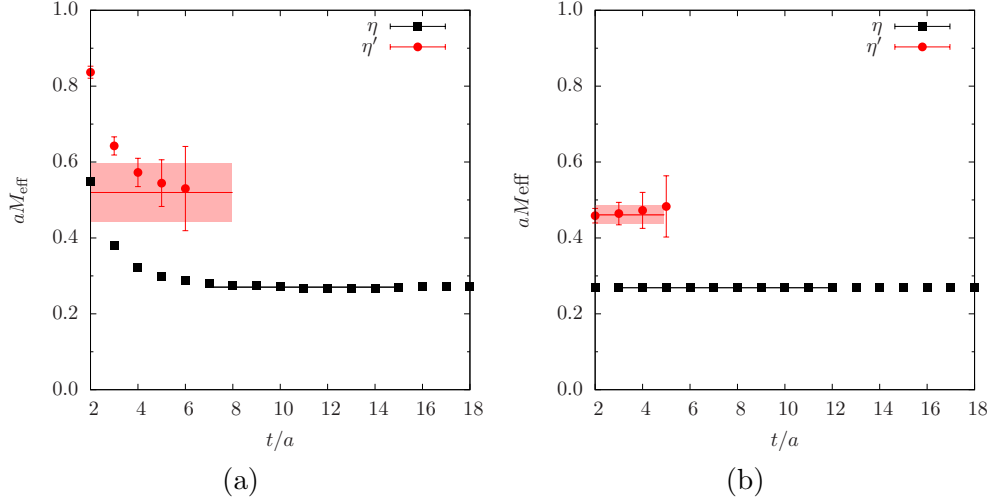


Fig. 2. Effective masses  $M_\eta^{\text{OS}}$  and  $M_{\eta'}^{\text{OS}}$  for the *A80.24s* ensemble using  $\eta_s$  matching for (a) a  $6 \times 6$  correlation matrix including local and fuzzed operators and (b) a  $3 \times 3$  local-only correlation matrix with connected excited states subtracted. The fitted values are shown as lines with error band. The corresponding fit range is indicated by the length of the lines. For further details see text and table A.7.

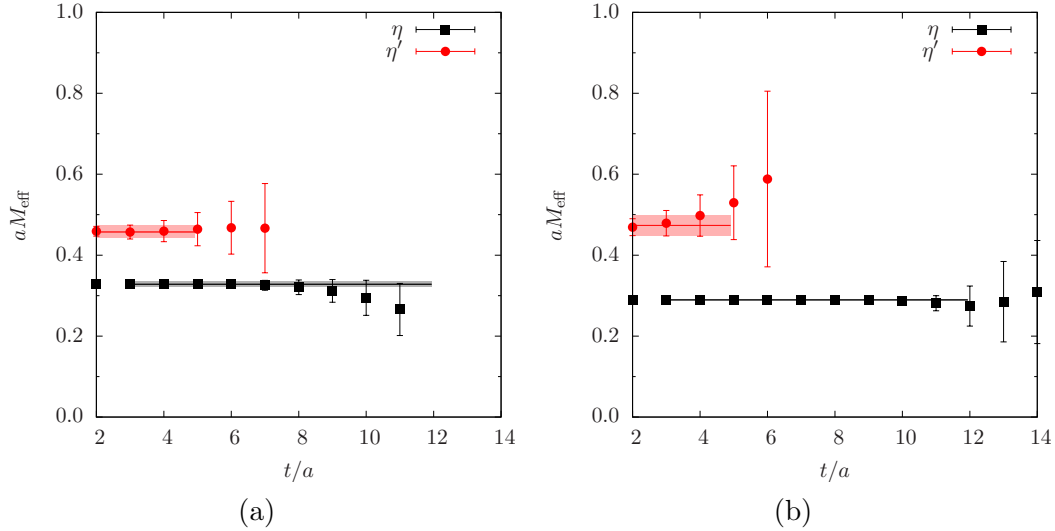


Fig. 3. We show the effective masses  $aM_\eta^{\text{OS}}$  and  $M_{\eta'}^{\text{OS}}$  from a  $3 \times 3$  correlation matrix after subtraction of excited states as described in the text for ensemble *A60.24*. Panel (a) is for kaon matching and (b) for  $\eta_s$  matching.

The  $\eta_c$  decouples from  $\eta$  and  $\eta'$  and the corresponding signal is lost in noise very early in  $t/a$ . Hence, we will not discuss it further here and due to the decoupling we will also not discuss the charm quark mass dependence of operators in the following.

It turns out that the choice of the matching variable makes a significant difference for the extracted value of  $M_\eta$ . Moreover, we always find  $aM_\eta^{\eta_s} < aM_\eta^K$ .

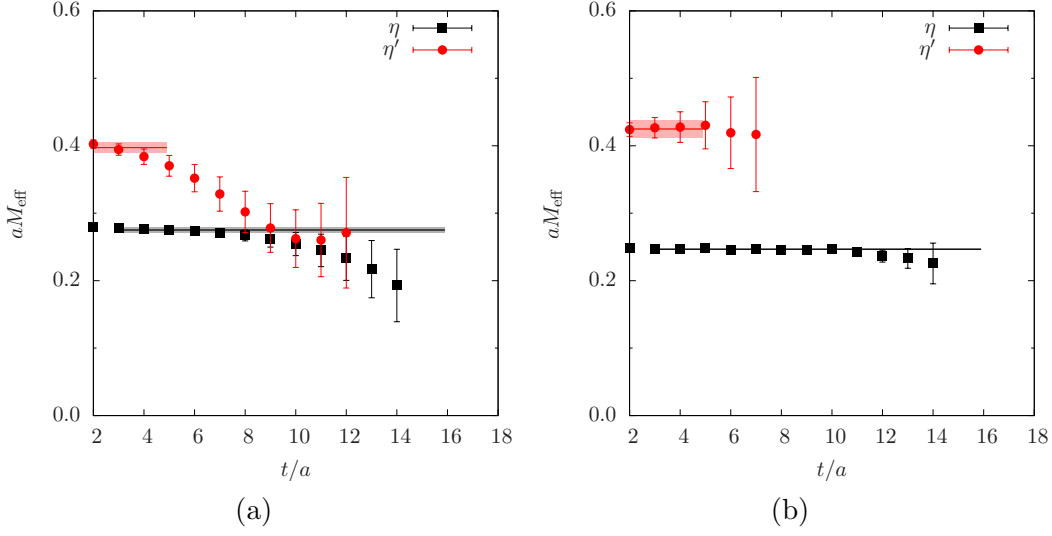


Fig. 4. We show the effective masses  $aM_\eta$  and  $M_{\eta'}$  of the two lowest-lying states on the  $B55.32$  ensemble for (a) kaon matching and (b) the unitary case using subtraction of excited states as described in the text.

On the other hand, the value of  $M_{\eta'}$  is unaffected within statistical errors. We find this consistently for all the ensembles investigated; cf. tables A.1 and A.2.

In addition one observes  $\phi^K < \phi^{\eta_s}$  by approximately  $15^\circ$ ; cf. table A.3. This results from a change in the overlap of mass and flavour eigenstates, leading to an increased light quark contribution to the  $\eta$  for kaon matching. Consequently, the light quark contribution to the  $\eta'$  is reduced, while the respective strange quark contributions behave in the opposite way. Since most of the noise is introduced by the light quark disconnected diagrams in our calculation, this explains why  $M_\eta^{\eta_s}$  in general exhibits a smaller statistical error than  $M_\eta^K$ , whereas the error for  $M_{\eta'}^{\eta_s}$  is larger than the one for  $M_{\eta'}^K$ .

However, there is a tendency that kaon matching leads to worse plateaus than  $\eta_s$  matching. A particularly extreme case of this behaviour is shown in figure 4 for the  $B55.32$  ensemble. In the left panel the effective masses for the two lowest lying states from kaon matching are plotted. Clearly there is no plateau visible for the first excited state. For comparison and to guide the eye we show the situation in the unitary setup in the right panel, calculated on the same set of configurations. This is the only ensemble for which we cannot identify a plateau for the  $\eta'$  safely. Therefore, we will not quote a value for the  $\eta'$  mass for  $B55.32$  and kaon matching.

Although the observed behaviour on  $B55.32$  can still be interpreted as a statistical fluctuation, it might – in principle – also be caused by unitarity violation. However, it is neither possible to verify nor exclude the latter from our present data. While earlier studies [6,51] observed a sign flip in the scalar correlator signalling unitarity violation at least for a certain regime of valence quark

masses, a similar argument cannot easily be extended to our case. The reason is that only the strange quark is treated in a mixed action approach while the light quarks are unitary. When looking at the scalar correlator made from strange quarks only, we do not observe it to become negative on any of our ensembles.

Another observation regarding the two matching methods concerns the behaviour of the ground states in the correlation functions used to build the full correlation function matrix. One expects all correlators with the same quantum numbers to asymptotically approach the same ground state mass. We observe this for the unitary case, where the  $\eta$  mass can be extracted from all correlators in the matrix  $\mathcal{C}$  (diagonal and off-diagonal) at large Euclidean times. In the OS case we observe a similar behaviour for  $\eta_s$  matching, but for kaon matching e.g. the strange-strange correlator alone does often not reproduce the  $\eta$  mass from the light-light correlator. This might signal unitarity violations for the kaon matching procedure on the one hand, and can explain the worse plateaus for this particular choice of the matching observable on the other hand.

Finally, for  $M_{\eta}^{\eta_s}$  we observe the error to be reduced approximately by a factor of two with respect to the unitary result for all ensembles (cf. table A.1). We attribute this to the fact that we can use the variance reduction method discussed in section 3.1 for the OS strange quark, which is not possible for the unitary strange quark. However, the errors of  $M_{\eta'}^{\eta_s}$  and  $\phi^{\eta_s}$  do not show such an error reduction (cf. table A.2 and A.3), presumably because the strange quark contributes little to these observables.

#### 4.1 Light Quark Mass Dependence

The first goal of this paper is to compare unitary to mixed action approaches and study the continuum limit of the corresponding differences. For this purpose we will study differences of quantities of the form  $\Delta O = O^{\text{OS}} - O^{\text{unitary}}$ . Our ensembles at different values of the lattice spacing are not at exactly identical light and strange sea quark masses. Therefore, we have to understand whether we can nevertheless study the continuum limit.

Theoretically, the answer to this question is yes: both in the unitary and in the mixed action approach we may write

$$O^{\text{lat}} = O^{\text{cont}} + \mathcal{O}(a^2 \Lambda_{\text{QCD}}^2)$$

and henceforth the aforementioned difference  $\Delta O$  is  $\mathcal{O}(a^2 \Lambda_{\text{QCD}}^2)$ . A quark mass dependence is expected to be negligible because for the quark mass difference  $\delta\mu \ll \Lambda_{\text{QCD}}$  holds. Since  $\Delta O$  is always computed on identical gauge config-

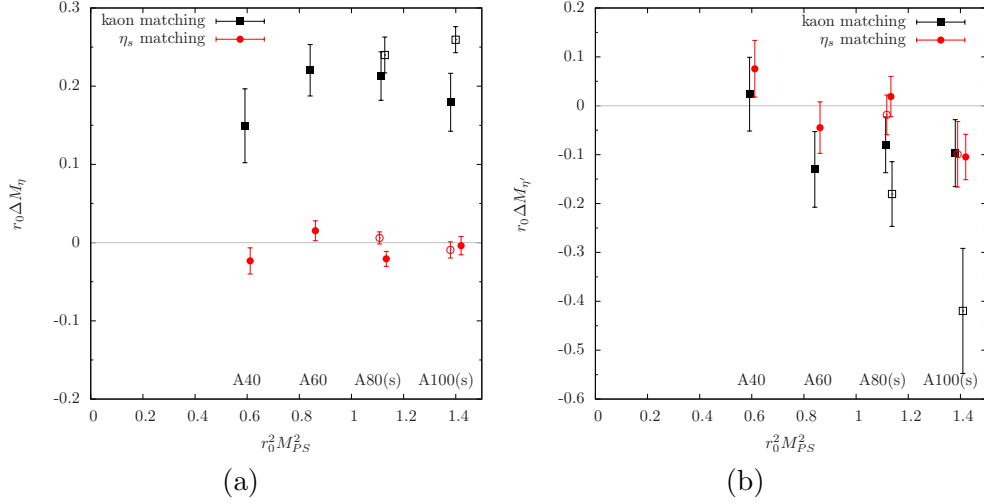


Fig. 5. (a)  $r_0 \Delta M_\eta$  as a function of  $(r_0 M_{PS})^2$  for the four A ensembles A40, A60, A80(s) and A100(s). Open symbols correspond to the s-ensembles. (b) like (a), but for  $r_0 \Delta M_{\eta'}$ . The kaon matching and s-ensemble data have been displaced horizontally for better legibility.

$\beta$	1.90	1.95	2.10
$r_0/a$	5.31(8)	5.77(6)	7.60(8)

Table 4

The chirally extrapolated values for  $r_0/a$  at each value of  $\beta$  corresponding to the three different lattice spacings [8].

urations there is no physical quark mass dependence that needs to be taken into account, because it cancels in the difference.

Despite this theoretical argument, let us also investigate this point numerically. We first study the light quark mass dependence of the difference between unitary and OS values of  $M_\eta$  and  $M_{\eta'}$ . For this purpose we focus on the A-ensembles A40, A60, A80 and A100, where we have different light quark mass values available. We denote

$$\Delta M_X = M_X^{\text{OS}} - M_X^{\text{unitary}}, \quad X = \eta, \eta'$$

the difference between unitary and OS meson masses. Analogously we define the angle difference  $\Delta\phi$ .  $r_0 \Delta M_\eta$  is shown for the A-ensembles in the left panel of figure 5 as a function of  $(r_0 M_{PS})^2$ . The chirally extrapolated values of  $r_0/a$  used in this study have been determined in [8] and are listed in table 4. Filled circles represent the  $\eta_s$  matching results, filled boxes the corresponding kaon matching results. The differences are computed using exactly the same configurations leading to reduced statistical errors due to the correlation between unitary and OS data.

For  $\eta_s$  matching  $r_0 \Delta M_\eta$  is for all four investigated ensembles compatible with zero within one sigma, while for kaon matching the difference is always positive



and not compatible with zero. For both matching procedures, but in particular for  $\eta_s$  matching, the dependence on  $(r_0 M_{\text{PS}})^2$  is not significant within our statistical uncertainties.

In the right panel of figure 5 we show  $r_0 \Delta M_{\eta'}$  as a function of  $(r_0 M_{\text{PS}})^2$ . Despite the larger uncertainties, the differences are compatible with zero for all ensembles and both matching procedures. There is a slight trend for differences with larger modulus for kaon matching. Like for the  $\eta$  the light quark mass dependence is not significant.

The angle difference  $\Delta\phi$  shows a very similar behaviour to  $\Delta M_{\eta}$ , see tables A.4 and A.5. For  $\eta_s$  matching the difference is compatible with zero, while for kaon matching a value of about  $-15^\circ$  is observed. Also here the light quark mass dependence is not significant. Besides, we find that the difference between  $\phi_\ell$  and  $\phi_s$  is compatible with zero for both matching methods and compatible to the one found in the unitary setup [19], again confirming the smallness of OZI suppressed corrections.

In order to check the strange quark mass dependence of the differences  $\Delta M$  and  $\Delta\phi$  we make use of the A80, A80s and A100, A100s ensembles. The s-ensembles differ from their non-s counterparts only by a different bare strange quark mass value. The corresponding values for the differences defined before are also displayed in figure 5 with open symbols. For  $\eta_s$  matching the differences show no dependence on the strange quark mass, whereas this cannot be concluded completely for kaon matching. In particular, we see for A100s deviations for kaon matching, but statistical errors can still account for the deviation.

## 4.2 Continuum Limit

Next, we study the dependence on the lattice spacing. For this purpose we use the ensembles A60.24, B55.32 and D45.32sc, which have approximately the same physical value of the pion mass, i.e.  $r_0 M_{\text{PS}}^{A60.24} = 0.917(14)_{\text{stat}}$ ,  $r_0 M_{\text{PS}}^{B55.32} = 0.888(09)_{\text{stat}}$  and  $r_0 M_{\text{PS}}^{D45.32sc} = 0.911(11)_{\text{stat}}$ , where we included the statistical error from the respective, chirally extrapolated values of  $r_0/a$ . As discussed in the previous section, we do not expect the residual differences in the light and strange quark masses to have any effect on this study.

The difference between OS and unitary results  $\Delta M$  for both matching procedures is shown for  $\eta$  and  $\eta'$  in figure 6 as a function of  $(a/r_0)^2$  in the left and right panel, respectively. The lines represent linear fits in  $(a/r_0)^2$  to our data, and the corresponding continuum extrapolated values are shown with open symbols.

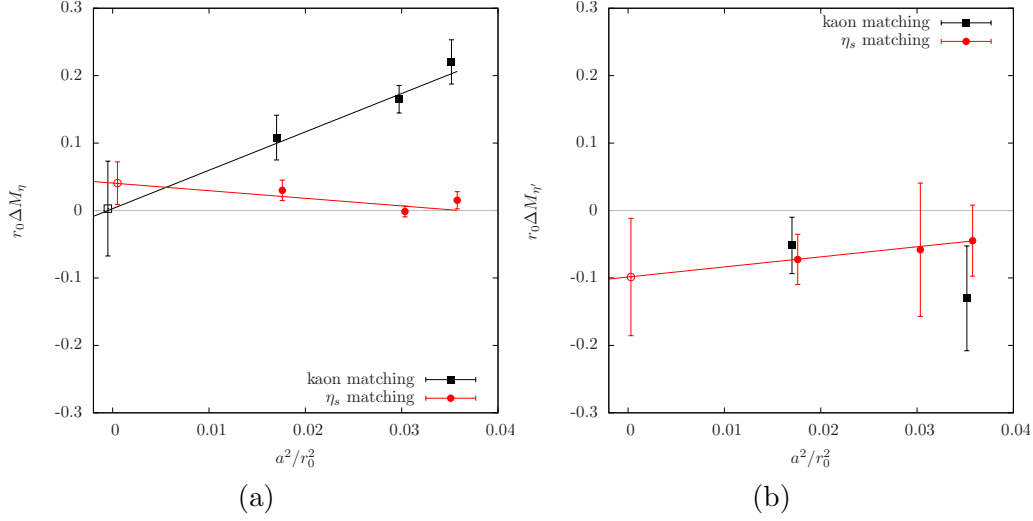


Fig. 6. Continuum extrapolation of (a)  $r_0 \Delta M_\eta$  and (b)  $r_0 \Delta M_{\eta'}$  as a function of  $(r_0/a)^2$ . We show the continuum extrapolated results from a linear extrapolation of the three ensembles ( $D45.32sc$ ,  $B55.32$ ,  $A60.24$ ) in  $(a/r_0)^2$  as open symbols. The continuum results are displaced horizontally for legibility.

$r_0 \Delta M_\eta$  is shown in the left panel of figure 6. For both matching procedures we observe a linear dependence in  $(a/r_0)^2$ . A corresponding continuum extrapolation in  $(a/r_0)^2$  leads to the expected vanishing of this difference at  $a = 0$  within errors. Kaon matching clearly exhibits larger  $a^2$  artifacts, while  $\eta_s$  matching gives  $r_0 \Delta M_\eta$  compatible with zero for each value of the lattice spacing separately.

In the right panel of figure 6 we show  $\Delta M_{\eta'}$ , again for both matching procedures. We remark that for kaon matching it is not possible to perform a fit from our present data, because of the missing mass value on the  $B55.32$  ensemble which is due to a bad plateau, as discussed above. In this case, statistical errors are significantly larger. However, within their larger errors the difference for the two matching procedures seems compatible and the difference vanishes in the continuum limit for  $\eta_s$  matching, as indicated by the fitted line in the plot. In contrast to the  $\eta$  mass, it cannot be concluded that lattice artifacts for kaon matching are significantly larger than for  $\eta_s$  matching.

In the left panel of figure 7  $\Delta\phi$  is shown as a function of  $(a/r_0)^2$ , again for the ensembles  $A60.24$ ,  $B55.32$  and  $D45.32sc$ . Like for  $\Delta M_\eta$  we observe also for  $\Delta\phi$  larger differences for kaon matching compared to  $\eta_s$  matching. For  $\eta_s$  matching the difference is in fact compatible with zero for all three ensembles separately. For both matching procedures the continuum extrapolated values are compatible with zero.

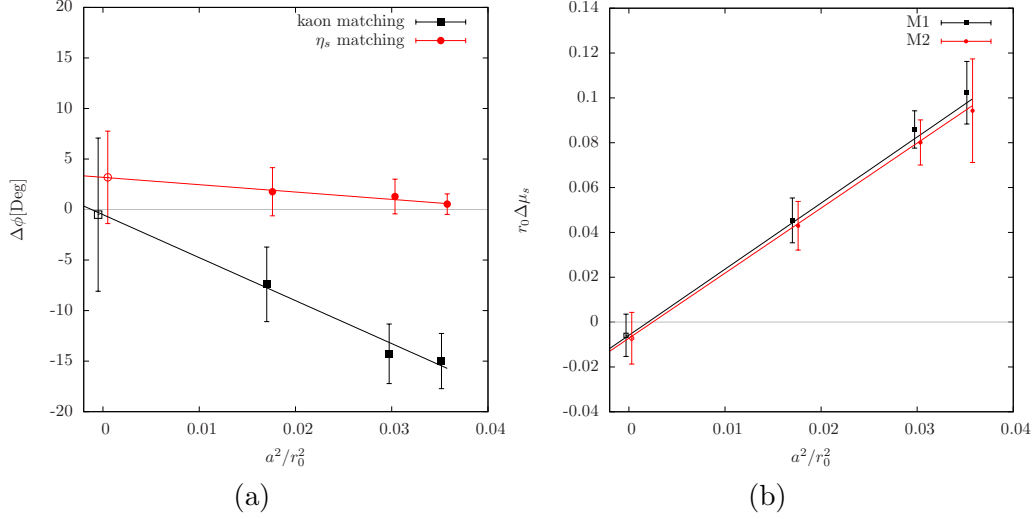


Fig. 7. (a) like figure 6, but for the mixing angle difference  $\Delta\phi$ . In (b) we show  $r_0\Delta\mu_s$  at 2 GeV in the  $\overline{\text{MS}}$  scheme as a function of  $(a/r_0)^2$  for the two methods M1 and M2 to estimate  $Z_P$  presented in Ref. [8].

Finally, we show in the right panel of figure 7 the quark mass difference

$$\Delta\mu_s = \frac{1}{Z_P}(\mu_s^K - \mu_s^{\eta_s}) \quad (19)$$

as a function of  $(a/r_0)^2$  for the three ensembles  $A60.24$ ,  $B55.32$  and  $D45.32sc$  at 2 GeV in the  $\overline{\text{MS}}$  scheme. The renormalisation constant  $Z_P$  has been taken from Ref. [8]. The two colours correspond to the methods M1 and M2 for estimating  $Z_P$ . We refer to Ref. [8] for the details. In the continuum limit it is expected that the two matching conditions agree and the difference should vanish like  $a^2$ . This is what is confirmed by figure 7 (b). Also, the two methods M1 and M2 give compatible results in the continuum limit, as expected.

#### 4.3 Dependence on Sea and Valence Strange Quark Mass

Next we study the dependence of the  $\eta$  (and in principle also the  $\eta'$ ) meson mass on the valence and sea quark mass values. As said in the introduction, the dependence on the valence and sea quark masses must be identical (at least within errors) to legitimate re-tuning in the valence quark masses only against sea strange quark mass mismatches. For this purpose we first define the dimensionless quantity

$$D_\eta^{\text{val}} = \frac{d(M_\eta^{\text{OS}})^2}{d(M_K^{\text{OS}})^2} \Big|_{\text{fixed sea ensemble}}, \quad (20)$$

which can be computed using the two matching points we have available for each ensemble. For estimating  $D_\eta^{\text{val}}$  from two  $\mu_s$  values at each ensemble, we

ensemble	$D_\eta^{\text{val}}$
A40.24	0.76(22)
A60.24	0.97(17)
A80.24	1.17(17)
A100.24	0.92(18)
A80.24s	1.07(11)
A100.24s	1.32(08)
B55.32	0.93(09)
D45.32sc	0.86(31)

Table 5

The valence derivative  $D_\eta^{\text{val}}$  obtained in the OS case by using the mass values from the kaon and  $\eta_s$  matching points.

ensemble	$D_\eta$	$D_\eta^{\text{OS}}$
A80/A80s	1.54(13)	1.37(07)
A100/A100s	1.34(15)	1.67(11)

Table 6

We list the values for  $D_\eta$  evaluated both for the unitary and the OS case using the two A80 and the two A100 ensembles. This derivative includes, in contrast to  $D_\eta^{\text{val}}$ , the valence and sea strange quark mass dependence. The values for  $D_\eta^{\text{OS}}$  are for  $\eta_s$  matching

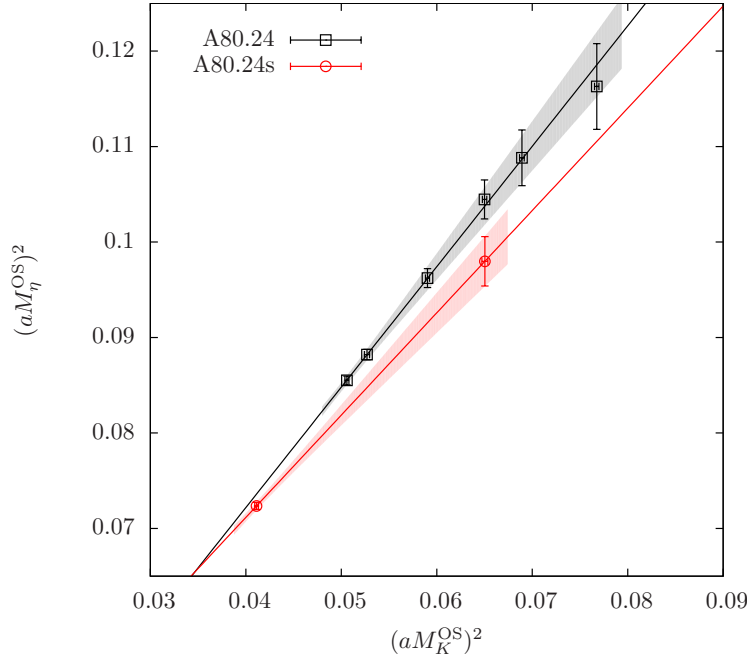


Fig. 8.  $(M_\eta^{\text{OS}})^2$  as a function of  $(M_K^{\text{OS}})^2$  for ensembles A80.24 and A80.24s.

have to assume that  $(M_\eta^{\text{OS}})^2$  depends linearly on  $(M_K^{\text{OS}})^2$  to a good approximation. That this is the case can be seen in figure 8, where we show  $(M_\eta^{\text{OS}})^2$  as a function of  $(M_K^{\text{OS}})^2$  for the two ensembles A80.24 and A80.24s. The lines represent linear fits to our data, which describe the data well within errors.

We expect  $D_\eta^{\text{val}}$  to be mostly sensitive to the valence strange quark mass if computed for several valence  $\mu_s$ -values on the same ensemble. The results for  $D_\eta^{\text{val}}$  are compiled in table 5 for all ensembles and  $\eta_s$  matching. They appear – independently of the lattice spacing, light and strange quark mass values – to be all compatible with 1. Taking the weighted average we obtain  $D_\eta^{\text{val}} = 1.09(5)$ , where the error is purely statistical. Concerning possible systematics we stress that there is no trend visible from the data, e.g. regarding a quark mass or lattice spacing dependence.

Including the sea strange quark mass dependence, the corresponding derivative is given by

$$D_\eta = \frac{d(M_\eta)^2}{d(M_K)^2}.$$

For the unitary case we find  $D_\eta = 1.45(10)$  and in the OS case  $D_\eta^{\text{OS}} = 1.46(6)$ , using the A100.24, A100.24s and A80.24, A80.24s ensembles and  $\eta_s$  matching, see table 6. While  $D_\eta$  and  $D_\eta^{\text{OS}}$  are compatible within errors, they differ significantly from  $D_\eta^{\text{val}}$ . For kaon matching the relative statistical errors on  $D_\eta^{\text{OS}}$  turn out to be at least a factor five larger than for  $\eta_s$  matching. Therefore, a meaningful statement regarding the compatibility of  $D_\eta^{\text{OS}}$  with  $D_\eta$  and  $D_\eta^{\text{val}}$  for kaon matching is not possible from our current data.

We take this as an indication that  $M_\eta$  is indeed a quantity with a significant sea strange quark mass dependence. Therefore, correcting for mismatches of the sea strange quark mass value in the valence sector only is not enough for  $M_\eta$ .

In principle, the difference between  $D_\eta$  and  $D_\eta^{\text{val}}$  that we found for a single lattice spacing could also be a lattice artifact. We do not think this is the case for two reasons: first, in Ref. [18] the value of  $D_\eta$  was used to correct a mismatch in the strange quark mass tuning for all three lattice spacings available. And we did not observe large cut-off effects introduced by this procedure. Second, also  $D_\eta^{\text{OS}}$  is merely independent of the lattice spacing. In fact, as the  $D_X$  are computed from differences and the leading lattice artifacts are independent of the quark mass, it is expected that these quantities are not plagued by large cut-off effects.

Unfortunately, the statistical uncertainty on the  $\eta'$  meson masses is too large to allow for a meaningful investigation of  $D_{\eta'}$ . Within errors this quantity is always zero, irrespective of whether the valence or the full strange quark mass dependence is considered. Moreover,  $M_{\eta'}$  has a larger light than strange quark contribution. It would, therefore, be interesting to perform the same study for the valence light quark mass instead of the valence strange.

Finally, we remark that it is in principle possible to calculate the difference between  $D_\eta$  and  $D_\eta^{\text{val}}$  from chiral perturbation theory [52,53,54]. At leading

order the corresponding prediction is  $4/3$  for both derivatives, implying that the difference is an NLO effect.

## 5 Summary and Discussion

In this paper we have studied  $\eta$  and  $\eta'$  mesons in a mixed action approach and in comparison to the unitary results. The mixed action was so-called Osterwalder-Seiler fermions on a twisted mass sea with  $N_f = 2 + 1 + 1$  dynamical quark flavours.

We have found that indeed the difference between mixed and unitary results vanishes as the continuum limit is approached. The rate is as expected of  $\mathcal{O}(a^2)$  [11] for all quantities and matching procedures investigated in this paper.

For the  $\eta$  mass we find a significant dependence of the size of the cutoff effects on the matching procedure. Lattice artifacts in the difference to the unitary result are compatible with zero when the two actions are matched using the  $\eta_s$  meson, while they are of normal size when the kaon is used as a matching variable. The same is true for the mixing angle and the strange quark mass.

For  $M_{\eta'}$  we do not observe a strong dependence on the matching procedure. This can have two reasons: first the error of  $M_{\eta'}$  is large making precise statements difficult. Second, the  $\eta'$  receives a strong contribution from sea quarks, because it is mainly the singlet state. The sea quark contributions are unaffected by different choices of the valence strange quark mass. Hence, this finding might reflect the physical properties of the  $\eta'$  meson.

This shows that the mixed action approach can also be applied in practice for flavour singlet quantities and, more generally, for observables involving fermionic disconnected diagrams. In case of  $\eta_s$  matching we find even reduced statistical errors for the  $\eta$  mass which might turn out to be an important advantage of the mixed approach. Thus, we will use the mixed action to investigate more complicated problems like  $\eta \rightarrow \gamma\gamma$  form factors or  $K\pi$  scattering for  $I = 1/2$  in the future.

Another important result of this paper is that for the  $\eta$  meson it is not sufficient to re-tune the valence quark masses to correct for small mismatches in the simulation runs. Our data shows that the valence strange quark mass dependence of the  $\eta$  differs significantly from the dependence on the sea plus valence strange quark mass. And this difference is not vanishing as the continuum limit is approached. For the  $\eta'$  we cannot make such a statement due to too large statistical errors, but we expect a similar result once  $M_{\eta'}$  can be

determined with higher accuracy.

The latter finding seems to contradict previous studies where the valence quark masses have been re-tuned to their physical values in the same mixed action approach for instance to determine non-singlet pseudo-scalar decay constants or quark masses (see for instance Refs. [8,55,56]). However, these investigations were concerned with observables for which the quark mass dependence is expected to be mainly governed by the valence quarks. For the  $\eta$  and  $\eta'$  mesons studied here this is not the case as OZI violating contributions are anomalously large. However, with high enough accuracy the effect seen here should also show up in other physical quantities, but on the current level of precision it is likely to be a negligible systematic uncertainty.

### *Acknowledgements*

We thank the members of ETMC for the most enjoyable collaboration. The computer time for this project was made available to us by the John von Neumann Institute for Computing (NIC) on the JUDGE, Jugene and Juqueen systems in Jülich. In particular we thank U.-G. Meißner for granting us access on JUDGE. We thank C. Michael and S. Simula for useful comments. We thank R. Frezzotti for useful discussions and very helpful comments on the draft of this paper. This project was funded by the DFG as a project in the SFB/TR 16 and in part by the Sino-German CRC110. Two of the authors (K.O. and C.U.) were supported by the Bonn-Cologne Graduate School (BCGS) of Physics and Astronomy. The open source software packages tmLQCD [57], Lemon [58] and R [59] have been used.

### **References**

- [1] O. Bär, G. Rupak, N. Shores, Simulations with different lattice Dirac operators for valence and sea quarks, Phys.Rev. D67 (2003) 114505. doi:10.1103/PhysRevD.67.114505.
- [2] H. Neuberger, Exactly massless quarks on the lattice, Phys.Lett. B417 (1998) 141–144. doi:10.1016/S0370-2693(97)01368-3.
- [3] H. Neuberger, More about exactly massless quarks on the lattice, Phys.Lett. B427 (1998) 353–355. doi:10.1016/S0370-2693(98)00355-4.
- [4] O. Bar, M. Golterman, Y. Shamir, Flavor symmetry breaking in lattice QCD with a mixed action, Phys.Rev. D83 (2011) 054501. doi:10.1103/PhysRevD.83.054501.

- [5] D. B. Kaplan, A Method for simulating chiral fermions on the lattice, *Phys.Lett.* B288 (1992) 342–347. doi:10.1016/0370-2693(92)91112-M.
- [6] K. Bowler, B. Joo, R. Kenway, C. Maynard, R. Tweedie, Lattice QCD with mixed actions, *JHEP* 0508 (2005) 003. doi:10.1088/1126-6708/2005/08/003.
- [7] K. Cichy, V. Drach, E. Garcia-Ramos, G. Herdoiza, K. Jansen, Overlap valence quarks on a twisted mass sea: a case study for mixed action Lattice QCD, *Nucl.Phys.* B869 (2013) 131–163. doi:10.1016/j.nuclphysb.2012.12.011.
- [8] N. Carrasco, et al., Up, down, strange and charm quark masses with  $N_f = 2+1+1$  twisted mass lattice QCD, *Nucl.Phys.* B887 (2014) 19–68. doi:10.1016/j.nuclphysb.2014.07.025.
- [9] W. A. Bardeen, A. Duncan, E. Eichten, N. Isgur, H. Thacker, Chiral loops and ghost states in the quenched scalar propagator, *Phys.Rev.* D65 (2001) 014509. doi:10.1103/PhysRevD.65.014509.
- [10] W. A. Bardeen, E. Eichten, H. Thacker, Chiral Lagrangian parameters for scalar and pseudoscalar mesons, *Phys.Rev.* D69 (2004) 054502. doi:10.1103/PhysRevD.69.054502.
- [11] R. Frezzotti, G. C. Rossi, Chirally improving Wilson fermions. II: Four-quark operators, *JHEP* 10 (2004) 070. doi:10.1088/1126-6708/2004/10/070.
- [12] R. Frezzotti, P. A. Grassi, S. Sint, P. Weisz, Lattice QCD with a chirally twisted mass term, *JHEP* 08 (2001) 058.
- [13] E. Witten, Current Algebra Theorems for the U(1) Goldstone Boson, *Nucl.Phys.* B156 (1979) 269. doi:10.1016/0550-3213(79)90031-2.
- [14] G. Veneziano, U(1) Without Instantons, *Nucl.Phys.* B159 (1979) 213–224. doi:10.1016/0550-3213(79)90332-8.
- [15] G. Veneziano, Goldstone Mechanism From Gluon Dynamics, *Phys.Lett.* B95 (1980) 90. doi:10.1016/0370-2693(80)90406-2.
- [16] E. B. Gregory, A. C. Irving, C. M. Richards, C. McNeile, Pseudoscalar flavor-singlets and staggered fermions, *PoS LAT2006* (2006) 176.
- [17] E. B. Gregory, A. C. Irving, C. M. Richards, C. McNeile, A study of the eta and eta' mesons with improved staggered fermions, *Phys.Rev.* D86 (2012) 014504. doi:10.1103/PhysRevD.86.014504.
- [18] K. Ottnad, et al.,  $\eta$  and  $\eta'$  mesons from  $N_f=2+1+1$  twisted mass lattice QCD, *JHEP* 1211 (2012) 048. doi:10.1007/JHEP11(2012)048.
- [19] C. Michael, K. Ottnad, C. Urbach,  $\eta$  and  $\eta'$  mixing from Lattice QCD, *Phys. Rev. Lett.* 111, 181602. doi:10.1103/PhysRevLett.111.181602.
- [20] G. Bennett, et al., Final Report of the Muon E821 Anomalous Magnetic Moment Measurement at BNL, *Phys.Rev.* D73 (2006) 072003. doi:10.1103/PhysRevD.73.072003.



- [21] T. Aoyama, M. Hayakawa, T. Kinoshita, M. Nio, Complete Tenth-Order QED Contribution to the Muon  $g-2$ , *Phys.Rev.Lett.* 109 (2012) 111808. doi:10.1103/PhysRevLett.109.111808.
- [22] M. Davier, A. Hoecker, B. Malaescu, Z. Zhang, Reevaluation of the Hadronic Contributions to the Muon  $g-2$  and to  $\alpha(M_Z)$ , *Eur.Phys.J. C* 71 (2011) 1515. doi:10.1140/epjc/s10052-012-1874-8, 10.1140/epjc/s10052-010-1515-z.
- [23] K. Hagiwara, R. Liao, A. D. Martin, D. Nomura, T. Teubner,  $(g-2)_\mu$  and  $\alpha(M_Z^2)$  re-evaluated using new precise data, *J.Phys. G* 38 (2011) 085003. doi:10.1088/0954-3899/38/8/085003.
- [24] K. Cichy, V. Drach, E. G. Ramos, K. Jansen, C. Michael, et al., Properties of pseudoscalar flavour-singlet mesons from 2+1+1 twisted mass lattice QCD, *PoS LATTICE2012* (2012) 151.
- [25] N. Christ, C. Dawson, T. Izubuchi, C. Jung, Q. Liu, et al., The  $\eta$  and  $\eta'$  mesons from Lattice QCD, *Phys.Rev.Lett.* 105 (2010) 241601. doi:10.1103/PhysRevLett.105.241601.
- [26] T. Kaneko, et al., Flavor-singlet mesons in  $N(f) = 2+1$  QCD with dynamical overlap quarks, *PoS LAT2009* (2009) 107.
- [27] J. J. Dudek, R. G. Edwards, B. Joo, M. J. Peardon, D. G. Richards, et al., Isoscalar meson spectroscopy from lattice QCD, *Phys.Rev. D* 83 (2011) 111502. doi:10.1103/PhysRevD.83.111502.
- [28] J. J. Dudek, R. G. Edwards, P. Guo, C. E. Thomas, Toward the excited isoscalar meson spectrum from lattice QCD, *Phys.Rev. D* 88 (9) (2013) 094505. doi:10.1103/PhysRevD.88.094505.
- [29] G. S. Bali, S. Collins, I. D'urr, Stephan an Kanamori,  $D_s \rightarrow \eta, \eta'$  semileptonic decay form factors with disconnected quark loop contributions, *Phys.Rev. D* 91 (1) (2015) 014503. arXiv:1406.5449, doi:10.1103/PhysRevD.91.014503.
- [30] R. Baron, et al., Light hadrons from lattice QCD with light (u,d), strange and charm dynamical quarks, *JHEP* 06 (2010) 111. doi:10.1007/JHEP06(2010)111.
- [31] R. Frezzotti, G. C. Rossi, Twisted-mass lattice QCD with mass non-degenerate quarks, *Nucl. Phys. Proc. Suppl.* 128 (2004) 193–202.
- [32] T. Chiarappa, F. Farchioni, K. Jansen, I. Montvay, E. Scholz, et al., Numerical simulation of QCD with u, d, s and c quarks in the twisted-mass Wilson formulation, *Eur.Phys.J. C* 50 (2007) 373–383. doi:10.1140/epjc/s10052-006-0204-4.
- [33] R. Frezzotti, G. C. Rossi, Chirally improving Wilson fermions. I:  $O(a)$  improvement, *JHEP* 08 (2004) 007.

- [34] K. Ottnad, Properties of pseudoscalar flavor singlet mesons from lattice QCD, Ph.D. thesis, University of Bonn, Bonn (February 2014).
- [35] B. Blossier, et al., Light quark masses and pseudoscalar decay constants from  $N_f=2$  Lattice QCD with twisted mass fermions, JHEP 04 (2008) 020. doi:10.1088/1126-6708/2008/04/020.
- [36] R. Frezzotti, G. Martinelli, M. Papinutto, G. Rossi, Reducing cutoff effects in maximally twisted lattice QCD close to the chiral limit, JHEP 0604 (2006) 038. doi:10.1088/1126-6708/2006/04/038.
- [37] R. Baron, et al., Computing K and D meson masses with  $N_f = 2+1+1$  twisted mass lattice QCD, Comput.Phys.Commun. 182 (2011) 299–316. doi:10.1016/j.cpc.2010.10.004.
- [38] A. Shindler, Twisted mass lattice QCD, Phys.Rept. 461 (2008) 37–110. doi:10.1016/j.physrep.2008.03.001.
- [39] K. Jansen, C. Michael, C. Urbach, The eta-prime meson from lattice QCD, Eur.Phys.J. C58 (2008) 261–269. doi:10.1140/epjc/s10052-008-0764-6.
- [40] P. Boucaud, et al., Dynamical Twisted Mass Fermions with Light Quarks: Simulation and Analysis Details, Comput.Phys.Commun. 179 (2008) 695–715. doi:10.1016/j.cpc.2008.06.013.
- [41] C. Alexandrou, M. Constantinou, V. Drach, K. Hadjiyiannakou, K. Jansen, et al., Evaluation of disconnected quark loops for hadron structure using GPUs, Comput.Phys.Commun. 185 (2014) 1370–1382. doi:10.1016/j.cpc.2014.01.009.
- [42] C. Michael, I. Teasdale, EXTRACTING GLUEBALL MASSES FROM LATTICE QCD, Nucl.Phys. B215 (1983) 433. doi:10.1016/0550-3213(83)90674-0.
- [43] M. Lüscher, U. Wolff, HOW TO CALCULATE THE ELASTIC SCATTERING MATRIX IN TWO-DIMENSIONAL QUANTUM FIELD THEORIES BY NUMERICAL SIMULATION, Nucl.Phys. B339 (1990) 222–252. doi:10.1016/0550-3213(90)90540-T.
- [44] B. Blossier, M. Della Morte, G. von Hippel, T. Mendes, R. Sommer, On the generalized eigenvalue method for energies and matrix elements in lattice field theory, JHEP 0904 (2009) 094. doi:10.1088/1126-6708/2009/04/094.
- [45] P. Lacey, A. McKerrell, C. Michael, I. M. Stopher, P. W. Stephenson, Efficient hadronic operators in lattice gauge theory, Phys. Rev. D51 (1995) 6403–6410.
- [46] R. Kaiser, H. Leutwyler, Pseudoscalar decay constants at large  $N(c)$ .
- [47] R. Kaiser, H. Leutwyler, Large  $N(c)$  in chiral perturbation theory, Eur.Phys.J. C17 (2000) 623–649. doi:10.1007/s100520000499.
- [48] T. Feldmann, P. Kroll, B. Stech, Mixing and decay constants of pseudoscalar mesons: The Sequel, Phys.Lett. B449 (1999) 339–346. doi:10.1016/S0370-2693(99)00085-4.

- [49] T. Feldmann, P. Kroll, B. Stech, Mixing and decay constants of pseudoscalar mesons, *Phys.Rev.* D58 (1998) 114006. doi:10.1103/PhysRevD.58.114006.
- [50] H. Neff, N. Eicker, T. Lippert, J. W. Negele, K. Schilling, On the low fermionic eigenmode dominance in QCD on the lattice, *Phys.Rev.* D64 (2001) 114509. doi:10.1103/PhysRevD.64.114509.
- [51] S. Prelovsek, C. Dawson, T. Izubuchi, K. Orginos, A. Soni, Scalar meson in dynamical and partially quenched two-flavor QCD: Lattice results and chiral loops, *Phys.Rev.* D70 (2004) 094503. doi:10.1103/PhysRevD.70.094503.
- [52] C. W. Bernard, M. F. Golterman, Chiral perturbation theory for the quenched approximation of QCD, *Phys.Rev.* D46 (1992) 853–857. doi:10.1103/PhysRevD.46.853.
- [53] S. R. Sharpe, N. Shoresh, Physical results from unphysical simulations, *Phys.Rev.* D62 (2000) 094503. doi:10.1103/PhysRevD.62.094503.
- [54] J. Bijnens, N. Danielsson, T. A. Lahde, Three-flavor partially quenched chiral perturbation theory at NNLO for meson masses and decay constants, *Phys.Rev.* D73 (2006) 074509. doi:10.1103/PhysRevD.73.074509.
- [55] N. Carrasco, P. Dimopoulos, R. Frezzotti, P. Lami, V. Lubicz, et al., Leptonic decay constants  $f_K, f_D$ , and  $f_{D_s}$  with  $N_f = 2 + 1 + 1$  twisted-mass lattice QCD, *Phys.Rev.* D91 (5) (2015) 054507. arXiv:1411.7908, doi:10.1103/PhysRevD.91.054507.
- [56] B. Blossier, et al., Pseudoscalar decay constants of kaon and D-mesons from  $N_f = 2$  twisted mass Lattice QCD, *JHEP* 0907 (2009) 043. doi:10.1088/1126-6708/2009/07/043.
- [57] K. Jansen, C. Urbach, tmLQCD: A Program suite to simulate Wilson Twisted mass Lattice QCD, *Comput.Phys.Commun.* 180 (2009) 2717–2738. doi:10.1016/j.cpc.2009.05.016.
- [58] A. Deuzeman, S. Reker, C. Urbach, Lemon: an MPI parallel I/O library for data encapsulation using LIME, *Comput.Phys.Commun.* 183 (2012) 1321–1335. arXiv:1106.4177, doi:10.1016/j.cpc.2012.01.016.
- [59] R Development Core Team, R: A language and environment for statistical computing, R Foundation for Statistical Computing, Vienna, Austria, ISBN 3-900051-07-0 (2005).  
URL <http://www.R-project.org>

## A Data Tables

In this appendix we have compiled all data in tables for convenience.

ensemble	$aM_\eta$	$aM_\eta^{\eta_s}$	$aM_\eta^K$
A40.24	0.2837(47)	0.2793(35)	0.312(12)
A60.24	0.2870(28)	0.2899(16)	0.3285(74)
A80.24	0.3009(20)	0.2970(09)	0.3410(67)
A100.24	0.3074(23)	0.3067(13)	0.3412(75)
A80.24s	0.2678(13)	0.2690(07)	0.3130(42)
A100.24s	0.2759(17)	0.2741(10)	0.3247(30)
B55.32	0.2467(12)	0.2465(07)	0.2753(34)
D45.32sc	0.1890(34)	0.1929(39)	0.2032(72)

Table A.1

Results for  $aM_\eta$  for the unitary and the mixed action approach. For the latter we show the values corresponding to  $\eta_s$  and kaon matching.

ensemble	$aM_{\eta'}$	$aM_{\eta'}^{\eta_s}$	$aM_{\eta'}^K$
A40.24	0.443(27)	0.457(28)	0.448(15)
A60.24	0.482(27)	0.474(27)	0.458(15)
A80.24	0.481(26)	0.485(29)	0.466(17)
A100.24	0.461(24)	0.441(21)	0.442(13)
A80.24s	0.465(23)	0.461(25)	0.431(13)
A100.24s	0.542(42)	0.523(40)	0.463(20)
B55.32	0.425(12)	0.415(12)	bad plateau
D45.32sc	0.278(12)	0.269(12)	0.271(09)

Table A.2

Same as table A.1, but for  $aM_{\eta'}$ .

ensemble	$\phi$	$\phi^{\eta_s}$	$\phi^K$
A40.24	47.1(2.0)	47.3(2.2)	30.6(4.1)
A60.24	49.2(1.4)	49.8(1.6)	34.2(3.7)
A80.24	49.9(1.1)	51.1(1.1)	38.0(3.5)
A100.24	49.6(1.3)	50.3(1.3)	31.9(4.1)
A80.24s	51.3(0.8)	52.6(0.5)	36.2(3.2)
A100.24s	53.8(0.7)	55.1(0.6)	44.2(2.7)
B55.32	48.2(0.8)	49.5(1.3)	34.0(2.9)
D45.32sc	45.6(2.5)	47.3(4.4)	38.2(5.8)

Table A.3

Same as table A.1, but for the mixing angle  $\phi$ .

ensemble	$a\Delta M_\eta$	$a\Delta M_{\eta'}$	$\Delta\phi[Deg]$
A40.24	+0.0281(89)	+0.004(14)	-16.5(2.6)
A60.24	+0.0415(61)	-0.024(15)	-15.0(2.7)
A80.24	+0.0401(58)	-0.015(11)	-11.9(2.6)
A100.24	+0.0338(69)	-0.018(13)	-17.7(3.3)
A80.24s	+0.0452(43)	-0.034(12)	-15.1(2.8)
A100.24s	+0.0489(31)	-0.079(24)	-9.5(2.7)
B55.32	+0.0286(35)	N/A	-14.3(2.9)
D45.32sc	+0.0142(44)	-0.007(06)	-7.4(3.7)

Table A.4

Values for  $a\Delta M_\eta$ ,  $a\Delta M_{\eta'}$  and  $\Delta\phi[Deg]$  as defined in the main text for kaon matching procedure.

ensemble	$a\Delta M_\eta$	$a\Delta M_{\eta'}$	$\Delta\phi[Deg]$
A40.24	-0.0044(32)	+0.014(11)	+0.2(1.2)
A60.24	+0.0029(24)	-0.008(10)	+0.5(1.0)
A80.24	-0.0039(18)	+0.004(08)	-1.2(0.6)
A100.24	-0.0007(22)	-0.020(09)	+0.7(1.0)
A80.24s	+0.0011(15)	-0.004(08)	+1.3(0.9)
A100.24s	-0.0018(20)	-0.019(13)	+1.3(0.8)
B55.32	-0.0002(14)	-0.010(17)	+1.3(1.5)
D45.32sc	+0.0039(20)	-0.010(05)	+1.8(2.4)

Table A.5

Same as table A.4, but for  $\eta_s$  matching procedure.

ensemble	$aM_K^K$	$aM_K^{\eta_s}$	$aM_{\eta_s}^K$	$aM_{\eta_s}^{\eta_s}$
A40.24	0.2583(16)	0.2031(17)	0.3824(13)	0.3046(18)
A60.24	0.2669(09)	0.2161(09)	0.3838(10)	0.3123(14)
A80.24	0.2770(06)	0.2297(06)	0.3860(08)	0.3126(12)
A100.24	0.2880(08)	0.2422(09)	0.3923(11)	0.3178(16)
A80.24s	0.2551(07)	0.2027(07)	0.3533(09)	0.2720(12)
A100.24s	0.2649(07)	0.2173(07)	0.3538(12)	0.2695(18)
B55.32	0.2280(04)	0.1893(04)	0.3221(04)	0.2640(06)
D45.32sc	0.1758(10)	0.1618(10)	0.2319(04)	0.2096(05)

Table A.6

OS kaon and  $\eta_s$  mass values for both matching procedures.

ensemble	$t_1^{\eta_\ell}$	$t_2^{\eta_\ell}$	$t_1^{\eta_s}$	$t_2^{\eta_s}$	$t_0^\eta$	$t_1^\eta$	$t_2^\eta$	$t_0^{\eta'}$	$t_1^{\eta'}$	$t_2^{\eta'}$
<i>A</i> -ensembles	12	22	12	22	1	3	12	1	2	5
<i>B</i> 55.32	15	25	15	25	1	3	16	1	2	5
<i>D</i> 45.32 <sub>sc</sub>	18	30	18	30	1	3	16	1	2	5
<i>A</i> 80.24 <sup>6×6</sup>					2	7	15	1	2	8

Table A.7

List of fit parameters.  $t_1^{\eta_{l,s}}$  and  $t_2^{\eta_{l,s}}$  define the fit intervals for the ground state of the connected correlation function in the light (strange) sector, which is required for the subtraction of excited states from the full correlator, before solving the GEVP for the resulting correlation function matrix. The  $t_0$  values for the GEVP used to determine the  $\eta$ ,  $\eta'$  states are given by  $t_0^{\eta,\eta'}$  whereas  $t_1^{\eta,\eta'}$ ,  $t_2^{\eta,\eta'}$  denote the respective fit ranges to the principal correlators. In the last row we give the parameters for the GEVP applied to the full 6x6 correlation function matrix of the *A*80.24 ensemble for the  $\eta_s$  matching case, as shown in the left panel of figure 2.